Proceedings of
A Symposium Commemorating the
Legacy, Works, and Life of
Sir Robert Stawell Ball
Upon the 100th Anniversary of
A Treatise on the Theory of Screws
July 9-11, 2000
University of Cambridge, Trinity College

On the Line Geometry of a Class of Tensegrity Structures

B. Knight[+]
Y. Zhang[*]
J. Duffy[*]
C. Crane[*]

Abstract

The line geometries of a family of tensegrity structures[1] which have been called skew prisms (anti-prisms, tensegrity prisms) with pairs of triangular, square, pentagonal, hexagonal…tops and bases are investigated. This is accomplished using the so-called quality index, with S-P-S connectors. It is remarkable that the quality index for each skew prism is zero, which means that it has instantaneous mobility. Further examination revealed that all the sets of connector-lines for each prism belong to a linear complex of lines within a 5-system of screws. Each of the sets of lines is reciprocal to a single screw. Adding ties along the diagonals of the skew prism faces can easily form reinforced skew prisms. Gabriel (1997) presents this high geometrical stability.

[+] Advanced Programs Engineer, Harris Corporation, Vienna, VA
[*] Center for Intelligent Machines, University of Florida

[1] Briefly, any tensegrity structure consists of ties and struts. No pair of struts touch and the end of each strut is connected to three non-coplanar ties, which are in tension. 'Tensegrity' is an abbreviation of tension and integrity.

Introduction

Figure 1 illustrates a family of tensegrity structures, which have been called skew prisms, anti-prisms and tensegrity prisms. These have been investigated by Tobie (1976), Kenner (1976) and Gabriel (1997).

The First column in Figure 1 shows a sequence of parallel prisms with parallel ties of fixed length. A relative anti-clockwise rotation can be achieved by rotating the top of each prism through α as shown in Figure 1 to yield what is called a corresponding right-handed tensegrity prism in the second column[2], which is completed by inserting struts on the diagonals of the skew quadrilaterals. Left-handed tensegrity prisms, which are simple corresponding, mirror images similarly by rotating the tops in a clockwise sense and by interchanging the ties and struts.

It is a remarkable result that α **is unique** for each **tensegrity prism** and is given by $\alpha = 90 - \frac{180}{n}$ where n is the number of sides in the upper or lower polygons. Hence $\alpha = 30$, 45, 54 and 60 degrees for the triangle, square, pentagon and hexagon tensegrity prisms. This result was derived by Kenner (1976) and it is based upon Tobie (1967). The value for α together with the size of the tops and bases together with their distance apart enables one to compute the length of the struts and ties, which defines a unique configuration for the tensegrity prism.

It is interesting to note that Gabriel (1997) goes on to describe the addition of ties to each of the above tensegrity prisms and in this way forms reinforced prisms. Such prisms have geometric rigidity whereas the tensegrity prisms (see column 2 of Figure 1) have some geometric deformability.

For ease of visualization a plan view of each tensegrity prism is drawn in the first column of Figure 2 with the top sides shorter than those of the respective bases. Corresponding reinforced prisms are shown in the second column.

The octahedron in Figure 2b has a total of 6 connectors (3 struts and 3 ties) connecting the top and the base. The corresponding reinforced octahedron has 3 additional ties (drawn in broken lines) so that there are 9 connectors.

The square tensegrity prism has a total of 8 connectors (4 struts and 4 ties) joining the top and the base. Clearly corresponding reinforced square tensegrity prisms could have 4 or even up to 8 additional ties, the complication increasing as the number of ties increases.

The pentagonal tensegrity prism has a total of 10 connectors (5 struts and 5 ties) joining the top and the base. A corresponding reinforced prism with 5 additional ties is drawn. The additional reinforced prisms could be constructed by using 10 and even up to 15 additional ties.

---

[2] Such structures have been called anti-prisms, tensegrity prisms, and simplexes (Chassagnoux, 1992). Here we use the term “tensegrity prisms”.

The hexagonal tensegrity prism has a total of 12 connectors (6 struts and 6 ties). A corresponding reinforced prism with 6 additional ties is drawn. Further reinforced prisms could be constructed by adding 12, 18, 24, 30 up to 36 ties.

The remainder of the discussion in this paper is directed solely to the geometry of the lines connecting the tops and the bases of the tensegrity prisms (column 2, Figure1) and of the reinforced prisms (column 2, Figure 2) and not to tensegrity structures in general. It is based on two previous papers, Hunt and McAree (1998) and Lee, Duffy and Hunt (1998). The authors consider that an examination of the geometry of the connector-lines sheds some new light on the important observations of Gabriel (1997).

Quality Index

The quality index (see Lee, Duffy and Keler (1996)), and Lee, Duffy and Hunt (1998)) is a measure of the geometrical stability of in-parallel devices which in three dimensions consist of a pair of rigid platforms connected by legs which are kinematic S-P-S connectors (S denotes ball-and-socket joint and P a sliding joint). One platform, the base is fixed and the other platform, the top has six degrees of freedom, which are realized by actuating six or more sliding joints.

It is important to recognize that the geometrical stability defined here is solely dependent upon the geometry of the legs or connector-lines and it is different to that defined by Gabriel (1997).

Figure 3 illustrates a plan view of an octahedral platform manipulator with six S-P-S connectors or legs. For this geometry there are a two concentric S joints at each of 3

connector-points in both the top and the base. The equilateral top platform with side **a** is drawn smaller than the base with side b for ease of visualization. The octahedron is drawn in what we define as a central configuration and it is an example of semi-regular Archimedean anti-prism, Pearce (1978).

The Jacobian matrix J is a 6x6 matrix, the columns of which are the normalized coordinates of the leg lines. It enables us to compute from the six actuated force inputs the wrench that the top delivers. When transposed, the Jacobian matrix relates the relative linear speeds of the six actuators to a given twist of the top. When the Jacobian matrix is singular (i.e. when its determinant is zero) the actuators can neither equilibrate a general wrench applied to the top, nor prevent a transitory uncontrollable movement of the top. In this situation, the top is free to twist with one or more freedoms when the actuators are locked. When the Jacobian matrix is singular the corresponding configuration of the manipulator is said to be special (Hunt and McAree (1997)).

On the other hand there is a configuration where the determinant of the Jacobian namely $\left|\det J\right|$ is maximum ($\left|\det Jm\right|$) and we will define a dimensionless quality index

$$\lambda = \left| \frac{\det J}{\det Jm} \right| \tag{1}$$

For the purpose of computing quality indices, the square, pentagon and hexagon can be modeled as redundant manipulators with 8, 10 and 12, S-P-S connectors, and the corresponding Jacobian matrices being 6x8, 6x10 and 6x12 (the columns, as before,

being the normalized coordinates of the 8, 10, and 12 connector-lines respectively). The quality index can be re-defined for redundant manipulators by

$$\lambda = \sqrt{\frac{\det\left|JJ^T\right|}{\det\left|JJ^T\right|_m}} \qquad (2)$$

(see Zhang and Duffy (1998)). This makes complete sense because by the Cauchy-Binet theorem $\det \boldsymbol{JJ}^T = \ )_1^2 +)_2^2 + \ldots +)_n^2$ has geometrical meaning. Each $)_i$ is simply the determinant of the 6x6 submatrices of J, which is a 6xn matrix. Clearly when n=6, (2) reduces to (1). It has been shown using the Grassmann-Cayley algebra (White and Whitely (11)) that, for a general octahedron, when the leg lengths are not normalized, detJ has dimension of (volume)^3 and it is directly related to the products of volumes of tetrahedra, which form the octahedron. Hence, detJ and $\det JJ^T$ have physical meaning.

The top of the octahedral platform will now be rotated parallel to the base through an angle ϕ about the z-axis, starting at the central configuration (ϕ=0) and the quality index λ_6 measured as function of ϕ as shown in Figure 5 (The computation of λ_6 is given in the Appendix[#]). Clearly, as the displacements proceed, the six leg lengths all vary. However, we can identify four key configurations. These are illustrated by Figures 5 (a), (b), (c) and (d) and are labeled in Figure 4 by (a), (b), (c) and (d).

[#] The subscript i in λ_i is simply a counter of the number of connector joining the base and the top. Further, the function λ_6 vs. ϕ is described in the range $0^0 \le \phi \le 180^0$ only; $-180^0 \le \phi \le 0^0$ is simply a mirror image.

For all these locations the leg lengths are AB, AE, BE, BF, CF, and CD. (At this stage the reader should ignore the broken lines.), and from Figures 5(a) and 5(b), $\alpha = \phi - 60$.

(i) For the central configuration, Figure 5(a), $\phi=0$, and from Figure 4, $\lambda_6 = 1$. This means that the semi-regular Archimedean anti-prism is the most geometrically stable.

(ii) For the aligned configuration, Figure 5(b), $\phi=60^0$ and from Figure 4, $\lambda_6 = 0.42$. The tie lines AE, BF and CD (see Figure 1) meet at a point. They would be parallel if triangles ABC and DEF were the same size. Here struts AD, BF and CD are added to form a tensegrity prism. Since this tensegrity prism is not in tensegrity the ties AE, BF, and CD must be replaced by struts.

(iii) For the tensegrity prism, Figure $5(c)$, $\phi=90^0$ and from Figure 4, $\lambda_6 = 0$. This means the tensegrity prism is at a special configuration. It has instantaneous mobility. This due solely to the geometrical arrangement of the six connector-lines and it is also obtained when all the ties are replaced by struts which is the same as locking all the six actuators of an octahedral platform device. Hunt and McAree (1997) and Hunt (1978) describe this geometrical arrangement of the six connector-lines (AE, AD, BE, BF, CF, CD) as belonging to a linear complex. Their moments about the z-axis are all the same and the top platform is free to twist about a screw of pitch **h**; the axis lies on the z-axis. This screw is reciprocal

to the six connector-lines. We could say that the tensegrity prism has lost geometrical stability but we would prefer to say it has instantaneous mobility. Further, the tensegrity prism is certainly stable. When $\phi = 90^0$ all the tie lengths are a minimum, see Kenner (1976). The prism is in a state of minimum potential energy and must therefore be stable (see also (iv) below). For the tensegrity prism, Figure 5(d), ϕ=120 and from Figure 4 $\lambda_6 = 0.22$. The ties in Figures $5(c)$ and 5(d) are all in tension and the struts are in compression. Figure $5(c)$ defines the lower bound of tensegrity for which the tie lengths are minimum. At this configuration the three struts pass through the centroid of the prism. It is useful to consider that the three connecting ties in Figure 5(d) were elastic and the top platform was held. When released from the crossover configuration it would spring back to the configuration shown in Figure $5(c)$, which is the configuration of minimum potential energy.

(iv) It is interesting, as Gabriel (1997) suggests, to add ties along the diagonals of the skew prism faces as illustrated by the 2nd column, Figure 2. The Jacobian matrix is now 6x9 and the quality index λ_9 is given by (2). (Details of its derivation are given in the Appendix.) This quality index is plotted as a function of ϕ in Figure 4, which varies in the range $0.74 \le \lambda_9 \le 1$ and there is no longer a special configuration when $\phi = 90^0$. For the reinforced tensegrity prism, it is clear that the three new tie lines AF, BD and CD do not belong to a linear complex. At this

lower bound the prism is now geometrically stable i.e. it does not have an instantaneous mobility.

This pattern of results extends to the square, pentagon, hexagon…tensegrity prisms. The corresponding key locations for the square tensegrity prism are illustrated by Figures 6(a), (b), (c) and (d), and are labeled in Figure 7 by (a), (b), (c) and (d).

(i) For the central configuration the semi-regular Archimedian anti-prism, Figure 6(a), $\phi = 0^0$ and $\lambda_8 = 1$.

(ii) For the aligned configuration, Figure 6(b), $\phi = 45^0$ and $\lambda_8 = 0.54$. The four ties AF, BG, CH and DE all meet at a point.

(iii) For the tensegrity prism, Figure 6(c), $\phi = 90^0$ and from Figure 7, $\lambda_8 = 0$. All the eight connector-lines now belong to a linear complex (see for example Hunt and McAree(1997)) and the top platform is free to twist instantaneously about a screw that lies on the z-axis. This is the configuration of minimum potential energy when the ties are elastic.

(iv) For the tensegrity prism, Figure 6(d), $\phi = 135^0$ and $\lambda_8 = 0.1$.

Figure 7 illustrates the results for a reinforced square tensegrity prism, for which 8 additional ties have been added to preserve symmetry. Here the quality index is the range $0.96 \le \lambda_6 \le 1$ for $-180^0 \le \phi \le 180^0$.

Conclusions

(i) The semi-regular Archimedean anti-prisms are the most stable.

(ii) Tensegrity prisms which are stable in the sense that they are configurations of minimum potential energy, but have instantaneous mobility simply because the connector-lines belong to a linear complex.

(iii) Reinforced tensegrity prisms are completely stable.

Appendix Determination of Quality Indices

Figure A1 illustrates the plan view of the moving platform ABC rotated ϕ_z about the z-axis, which is drawn through the reference point O normal to ABC. The x and y coordinates of the vertices A, B, and C are

$$x_A=r\cos(\phi_z+30^0), \qquad y_A=r\sin(\phi_z+30^0),$$
$$x_B=-r\cos(\phi_z-30^0), \qquad y_B=-r\sin(\phi_z-30^0),$$
$$x_C=r\sin\phi_z, \qquad y_C=-r\cos\phi_z \tag{A1}$$

where $r=\frac{a}{\sqrt{3}}$. From (A1)

$$x_A+x_B+x_C=0,$$
$$y_A+y_B+y_C=0. \tag{A2}$$

The complete set of coordinates of points A, B, C and D, E, F are therefore

$$A(x_A,y_A,z_A),B(x_B,y_B,z_B),C(x_C,y_C,z_C)$$
$$D\left(\frac{b}{2},-\frac{b}{2\sqrt{3}},0\right),E\left(0,\frac{b}{\sqrt{3}},0\right),F\left(-\frac{b}{2},-\frac{b}{2\sqrt{3}},0\right) \tag{A3}$$

where z is the height of the moving triangle ABC above the base triangle DEF.

Now the coordinates of a line joining two finite points with coordinates (x_1,y_1z_1) and (x_2,y_2,z_2) are given by the six second-order determinants of the array

$$\begin{bmatrix} 1 & x_1 & y_1 & z_1 \\ 1 & x_2 & y_2 & z_2 \end{bmatrix} \tag{A4}$$

The direction ratios of the line are

$$\mathrm{L}=\begin{vmatrix} 1 & x_1 \\ 1 & x_2 \end{vmatrix}, \quad \mathrm{M}=\begin{vmatrix} 1 & y_1 \\ 1 & y_2 \end{vmatrix}, \quad \mathrm{N}=\begin{vmatrix} 1 & z_1 \\ 1 & z_2 \end{vmatrix} \tag{A5}$$

And the moments of the line segment about the three coordinate axes are

$$\mathrm{P}=\begin{vmatrix} y_1 & z_1 \\ y_2 & z_2 \end{vmatrix}, \ \mathrm{Q}=\begin{vmatrix} z_1 & x_1 \\ z_2 & x_2 \end{vmatrix}, \ \mathrm{R}=\begin{vmatrix} x_1 & y_1 \\ x_2 & y_2 \end{vmatrix}. \tag{A6}$$

The coordinates of the line $\$_1$ are obtained using the coordinates of points D and A in (A7) to yield

$$\begin{bmatrix} 1 & \frac{b}{2} & -\frac{b}{2\sqrt{3}} & 0 \\ 1 & x_A & y_A & z \end{bmatrix} \tag{A7}$$

and for the AD leg

$$\hat{S}_1^T = \left[\left(x_A - \frac{b}{2} \right), \left(y_A + \frac{b}{2\sqrt{3}} \right), z; -\frac{bz}{2\sqrt{3}}, -\frac{bz}{2}, \frac{b}{2}\left(\frac{x_A}{\sqrt{3}} + y_A \right) \right] \tag{A8}$$

for the AE leg

$$\hat{S}_2^T = \left[x_A, \left(y_A - \frac{b}{\sqrt{3}} \right), z; \frac{bz}{\sqrt{3}}, 0, -\frac{bx_A}{\sqrt{3}} \right]. \tag{A9}$$

For the BE leg

$$\hat{S}_3^T = \left[x_B, \left(y_B - \frac{b}{\sqrt{3}} \right), z; \frac{bz}{\sqrt{3}}, 0, -\frac{bx_B}{\sqrt{3}} \right]. \tag{A10}$$

For the BF leg

$$\hat{S}_4^T = \left[\left(x_B + \frac{b}{2} \right), \left(y_B + \frac{b}{2\sqrt{3}} \right), z; -\frac{bz}{2\sqrt{3}}, \frac{bz}{2}, \frac{b}{2}\left(\frac{x_B}{\sqrt{3}} - y_B \right) \right]. \tag{A11}$$

For the CF leg

$$\hat{S}_5^T = \left[\left(x_C + \frac{b}{2} \right), \left(y_C + \frac{b}{2\sqrt{3}} \right), z; -\frac{bz}{2\sqrt{3}}, \frac{bz}{2}, \frac{b}{2}\left(\frac{x_C}{\sqrt{3}} - y_C \right) \right]. \tag{A12}$$

For the CD leg

$$\hat{S}_6^T = \left[\left(x_C - \frac{b}{2} \right), \left(y_C + \frac{b}{2\sqrt{3}} \right), z; -\frac{bz}{2\sqrt{3}}, -\frac{bz}{2}, \frac{b}{2}\left(\frac{x_C}{\sqrt{3}} + y_C \right) \right] \tag{A13}$$

It should be noted that the notation $\hat{S}_i^T = [S_i; S_{oi}]$ has been introduced. The above coordinates are not normalized and each row must be divided by $_i = \sqrt{S_i, S_i}$.

It follows that

$$\text{detJ} = \frac{1}{_1 \; _2 \; _3 \; _4 \; _5 \; _6} \qquad \left| \hat{S}_1 \hat{S}_2 \hat{S}_3 \hat{S}_4 \hat{S}_5 \hat{S}_6 \right| \tag{A14}$$

And the quality index for 6 connectors is given by

$$\lambda_6 = \frac{\det J}{\det J_m} \tag{A15}$$

where $\det J_m = \det J$ is evaluated at $\phi = 0^0$

For a reinforced prism we introduce ties AF, BD, CE and the coordinates for the corresponding lines $\$_7$, $\$_8$, and $\$_9$ are given by

$$\hat{S}_7 = \left[x_A + \frac{b}{2}, y_A + \frac{b}{2\sqrt{3}}, z; -\frac{bz}{2\sqrt{3}}, \frac{bz}{2}, \frac{b}{2}\left(\frac{x_A}{\sqrt{3}} - y_A \right) \right]$$

$$\hat{S}_8 = \left[x_B - \frac{b}{2}, y_B + \frac{b}{2\sqrt{3}}, z; -\frac{bz}{2\sqrt{3}}, -\frac{bz}{2}, \frac{b}{2}\left(\frac{x_B}{\sqrt{3}} - y_B \right) \right]$$

$$\hat{S}_9 = \left[x_C, y_C - \frac{b}{\sqrt{3}}, z; \frac{bz}{\sqrt{3}}, 0, -\frac{bz_c}{\sqrt{3}} \right] \tag{A16}$$

Now

$$J = \frac{1}{1 \quad 2 \cdots \quad 9} \left[\hat{S}_1 \hat{S}_2 \hat{S}_3 \ldots \hat{S}_8 \hat{S}_9 \right] \tag{A17}$$

and the quality index for 9 connectors is given by

$$\lambda_9 = \sqrt{\frac{\left| \mathrm{JJ}^{\mathrm{T}} \right|}{\left| \mathrm{JJ}^{\mathrm{T}} \right|_{\mathrm{m}}}} \tag{A18}$$

where $\left| JJ^T \right|_m$ is evaluated at $\phi=0^0$.

Figure A2 illustrates the plan view of the moving platform ABCD rotated ϕ_z about the z-axis, which is drawn through the reference point O normal to ABCD. The *x* and *y* coordinates of the vertices A, B, C, and D are

$$\begin{aligned} \mathrm{x_A} &= \mathrm{r}\cos\phi_{\mathrm{Z}}, & \mathrm{y_A} &= \mathrm{r}\sin\phi_{\mathrm{Z}}, \\ \mathrm{x_B} &= -\mathrm{r}\sin\phi_{\mathrm{Z}}, & \mathrm{y_B} &= \mathrm{r}\cos\phi_{\mathrm{Z}}, \\ \mathrm{x_C} &= -\mathrm{r}\cos\phi_{\mathrm{Z}}, & \mathrm{y_C} &= -\mathrm{r}\sin\phi_{\mathrm{Z}}, \\ \mathrm{x_D} &= \mathrm{r}\sin\phi_{\mathrm{Z}}, & \mathrm{y_D} &= -\mathrm{r}\cos\phi_{\mathrm{Z}} \end{aligned} \tag{A19}$$

where $r = \frac{a}{\sqrt{2}}$. From (A20)

$$\begin{aligned} x_A + x_B + x_C + x_D &= 0, \\ y_A + y_B + y_C + y_D &= 0. \end{aligned} \tag{A20}$$

The complete set of coordinates of points A, B, C, D and E, F, G, H are therefore

$$\begin{aligned} &A(x_A \quad y_A \quad z), \; B(x_B \quad y_B \quad z), \; C(x_C \quad y_C \quad z), \; D(x_D \quad y_D \quad z), \\ &E\left(\frac{b}{2} \quad -\frac{b}{2} \quad 0\right), \; F\left(\frac{b}{2} \quad \frac{b}{2} \quad 0\right), \; G\left(-\frac{b}{2} \quad \frac{b}{2} \quad 0\right), \; H\left(-\frac{b}{2} \quad -\frac{b}{2} \quad 0\right) \end{aligned} \tag{A21}$$

where z is the height of the moving square ABCD above the base square EFGH.

Similar to the triangle platform case, the coordinates of the line $\$_1$ are obtained using the coordinates of points E and A in (A23) to yield

$$\begin{bmatrix} 1 & \frac{b}{2} & -\frac{b}{2} & 0 \\ 1 & x_A & y_A & z \end{bmatrix} \tag{A22}$$

and for the AE leg

$$\widehat{S}_1^T = \left[(x_A - \frac{b}{2}), \quad (y_A - \frac{b}{2}), \quad z; \quad -\frac{bz}{2}, \quad -\frac{bz}{2}, \quad \frac{b(x_A + y_A)}{2} \right]. \tag{A23}$$

For the AF leg

$$\widehat{S}_2^T = \left[(x_A - \frac{b}{2}), \quad (y_A - \frac{b}{2}), \quad z; \quad \frac{bz}{2}, \quad -\frac{bz}{2}, \quad -\frac{b(x_A - y_A)}{2} \right]. \tag{A24}$$

For the BF leg

$$\widehat{S}_3^T = \left[(x_B - \frac{b}{2}), \quad (y_B - \frac{b}{2}), \quad z; \quad \frac{bz}{2}, \quad -\frac{bz}{2}, \quad -\frac{b(x_B - y_B)}{2} \right]. \tag{A25}$$

For the BG leg

$$\widehat{S}_4^T = \left[(x_B + \frac{b}{2}), \quad (y_B - \frac{b}{2}), \quad z; \quad \frac{bz}{2}, \quad \frac{bz}{2}, \quad -\frac{b(x_B + y_B)}{2} \right]. \tag{A26}$$

For the CG leg

$$\widehat{S}_5^T = \left[(x_C + \frac{b}{2}), \quad (y_C - \frac{b}{2}), \quad z; \quad \frac{bz}{2}, \quad \frac{bz}{2}, \quad -\frac{b(x_C + y_C)}{2} \right]. \tag{A27}$$

For the CH leg

$$\widehat{S}_6^T = \left[(x_C + \frac{b}{2}), \quad (y_C + \frac{b}{2}), \quad z; \quad -\frac{bz}{2}, \quad \frac{bz}{2}, \quad \frac{b(x_C - y_C)}{2} \right]. \tag{A28}$$

For the DH leg

$$\widehat{S}_7^T = \left[(x_D + \frac{b}{2}), \quad (y_D + \frac{b}{2}), \quad z; \quad -\frac{bz}{2}, \quad \frac{bz}{2}, \quad \frac{b(x_D - y_D)}{2} \right]. \tag{A29}$$

For the DE leg

$$\widehat{S}_8^T = \left[(x_D - \frac{b}{2}), \quad (y_D + \frac{b}{2}), \quad z; \quad -\frac{bz}{2}, \quad -\frac{bz}{2}, \quad \frac{b(x_D + y_D)}{2} \right]. \tag{A30}$$

It should be noted that the notation $\widehat{S}_i^T = [S_i; S_{oi}]$ has been introduced. The above coordinates are not normalized and each row must be divided by $l_i = \|S_i\|$.

It follows that

$$\mathbf{J} = \frac{1}{l_1 l_2 \cdots l_8} \left[\widehat{S}_1 \quad \widehat{S}_2 \quad \cdots \quad \widehat{S}_8 \right] \tag{A31}$$

and the quality index for 8 connectors is given by

$$\lambda_8 = \sqrt{\frac{\left|\mathbf{J}\mathbf{J}^{\mathrm{T}}\right|}{\left|\mathbf{J}\mathbf{J}^{\mathrm{T}}\right|_m}} \tag{A32}$$

where $\left|\mathbf{J}\mathbf{J}^{\mathrm{T}}\right|_m$ is evaluated at $\phi = 0°$.

For a reinforced prism we introduce ties AG, BH, CE, DF, AH, BE, CF, DG and the coordinates for the corresponding lines \$9, \$10, \$11, \$12, \$13, \$14, \$15, and \$16 are given by

$$\widehat{S}_9^T = \left[(x_A + \frac{b}{2}), \quad (y_A - \frac{b}{2}), \quad z; \quad \frac{bz}{2}, \quad -\frac{bz}{2}, \quad \frac{b(x_A + y_A)}{2}\right], \tag{A33}$$

$$\widehat{S}_{10}^T = \left[(x_B + \frac{b}{2}), \quad (y_B + \frac{b}{2}), \quad z; \quad -\frac{bz}{2}, \quad \frac{bz}{2}, \quad \frac{b(x_B - y_B)}{2}\right], \tag{A34}$$

$$\widehat{S}_{11}^T = \left[(x_C - \frac{b}{2}), \quad (y_C + \frac{b}{2}), \quad z; \quad -\frac{bz}{2}, \quad -\frac{bz}{2}, \quad \frac{b(x_C + y_C)}{2}\right], \tag{A35}$$

$$\widehat{S}_{12}^T = \left[(x_D - \frac{b}{2}), \quad (y_D - \frac{b}{2}), \quad z; \quad \frac{bz}{2}, \quad -\frac{bz}{2}, \quad -\frac{b(x_D - y_D)}{2}\right], \tag{A36}$$

$$\widehat{S}_{13}^T = \left[(x_A + \frac{b}{2}), \quad (y_A + \frac{b}{2}), \quad z; \quad -\frac{bz}{2}, \quad \frac{bz}{2}, \quad \frac{b(x_A - y_A)}{2}\right], \tag{A37}$$

$$\widehat{S}_{14}^T = \left[(x_B - \frac{b}{2}), \quad (y_B + \frac{b}{2}), \quad z; \quad -\frac{bz}{2}, \quad -\frac{bz}{2}, \quad \frac{b(x_B + y_B)}{2}\right], \tag{A38}$$

$$\widehat{S}_{15}^T = \left[(x_C - \frac{b}{2}), \quad (y_C - \frac{b}{2}), \quad z; \quad \frac{bz}{2}, \quad -\frac{bz}{2}, \quad -\frac{b(x_C - y_C)}{2}\right], \tag{A39}$$

$$\widehat{S}_{16}^T = \left[(x_D + \frac{b}{2}), \quad (y_D - \frac{b}{2}), \quad z; \quad \frac{bz}{2}, \quad \frac{bz}{2}, \quad -\frac{b(x_D + y_D)}{2}\right]. \tag{A40}$$

Now

$$\mathbf{J} = \frac{1}{l_1 l_2 \cdots l_{16}} \begin{bmatrix} \hat{S}_1 & \hat{S}_2 & \cdots & \hat{S}_{16} \end{bmatrix} \tag{A42}$$

and the quality index for 16 connectors is given by

$$\lambda_{16} = \sqrt{\frac{\left|\mathbf{J}\mathbf{J}^{\mathbf{T}}\right|}{\left|\mathbf{J}\mathbf{J}^{\mathbf{T}}\right|_m}} \tag{A43}$$

where $\left|\mathbf{J}\mathbf{J}^{\mathbf{T}}\right|_m$ is evaluated at $\phi = 0°$.

Acknowledgements

The authors wish to acknowledge the financial support of the Air Force Office of Scientific Research, Grant No. F49620-00-1-0021, the Air Force Research Laboratory, Tyndall AFB, Grant No. F08637-99-C-6008 and the Harris Corporation, Melbourne Florida, Grant No. 0244-9806976.

References

Chassagnoux, A., Chomarat, A., and Savel, J., (1992), "A Study of Morphological Characteristics of Tensegrity Structures," The International Journal of Space Structures, Vol. 7, No. 2, pp. 165-172.

Gabriel, J.F., (1997), "Beyond the Cube. The Architecture of Space Frames and Polyhedra," John Wiley and Sons, pp.390-400.

Hunt, K.H. and McAree, P.R., (1998), "The Octahedral Manipulator: Geometry and Mobility," International Journal of Robotic Research, Vol. 17, No. 8.

Hunt, K.H. (1978), “Kinematic Geometry of Mechanisms,” Oxford University Press

Kenner, H., (1976), “Geodesic Math and How to Use It,” University of California Press, Berkeley and Los Angeles, California.

Lee, J., Duffy, J., and Keler, M. (1996), “The Optimum Quality Index for the Stability of In-parallel Planar Platform Devices,” Proc. Of the ASME Design Technical Conferences, Published on CD-ROM 96-DETC/MECH-1135.

Lee, J., Duffy, J., and Hunt, K., (1998), “A Practical Quality Index Based on the Octahedral Manipulator,” The International Journal of Robotics Research, Vol. 17, No. 10, pp. 1081-1090.

Pearce, P., (1978), “Structure in Nature is a Strategy for Design,” MIT Press.

Tobie, S.T., (1967), “A Report on an Inquiry into The Existence, Formation and Representation of Tensile Structures,” Master of Industrial Design, Pratt Institute.

Parallel Prisms

Tensegrity Prisms

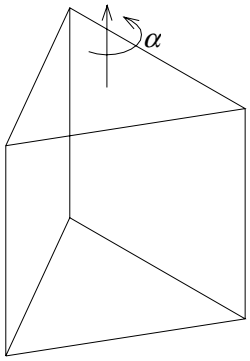

(a)

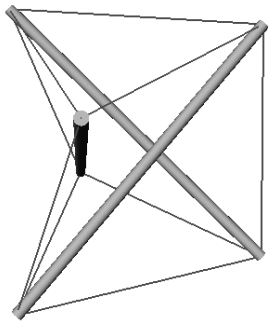

(b)

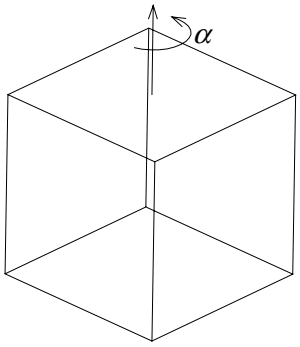

(c)

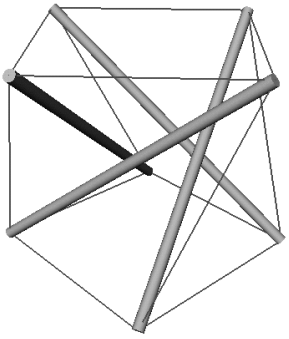

(d)

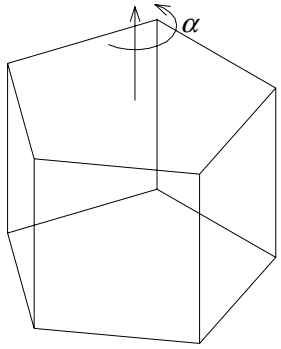

(e)

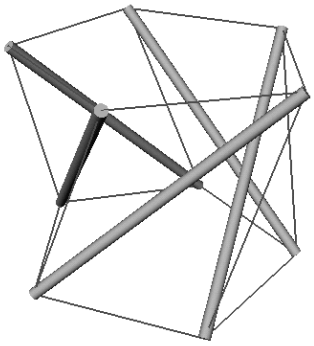

(f)

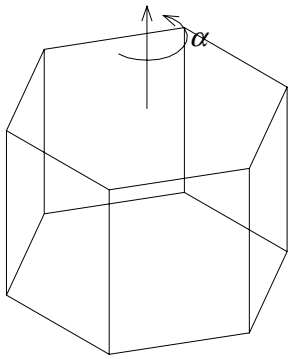

(g)

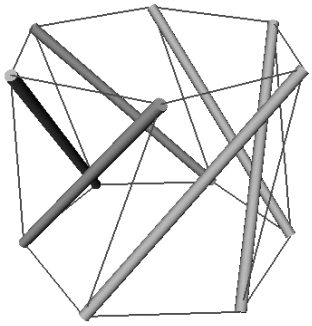

(h)

Figure 1: Tensegrity prisms

Tensegrity Prisms

Reinforced Tensegrity Prisms

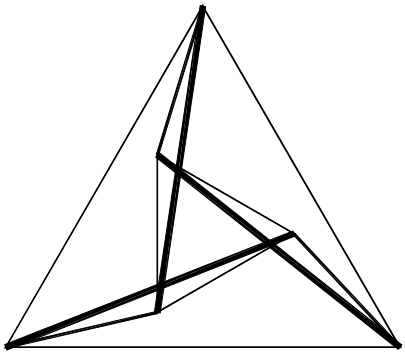

(a)

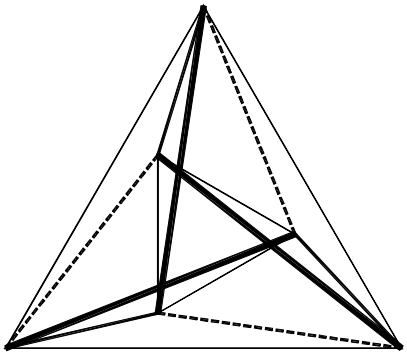

(b)

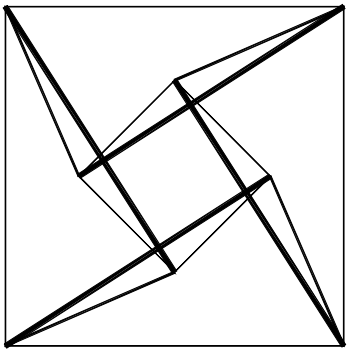

(c)

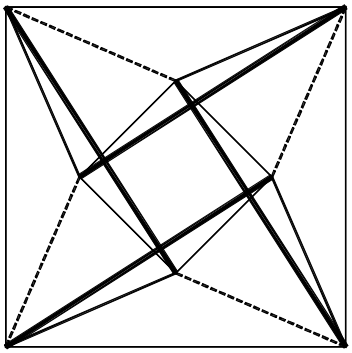

(d)

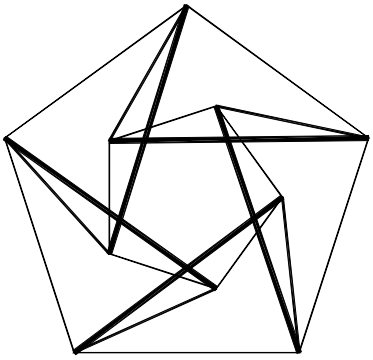

(e)

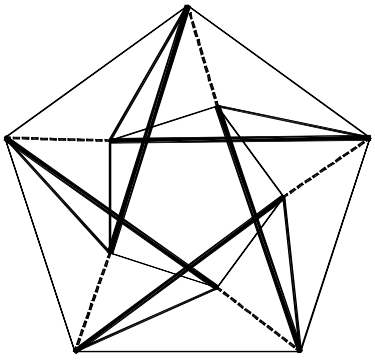

(f)

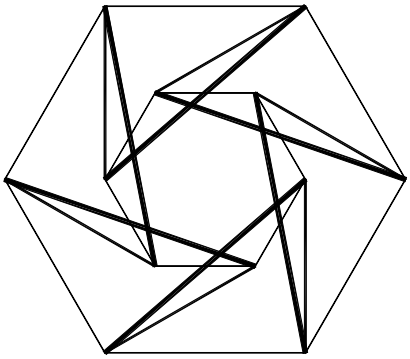

(g)

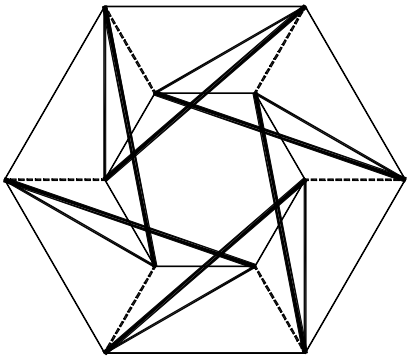

(h)

Figure 2: Plan view of tensegrity and corresponding reinforced prisms

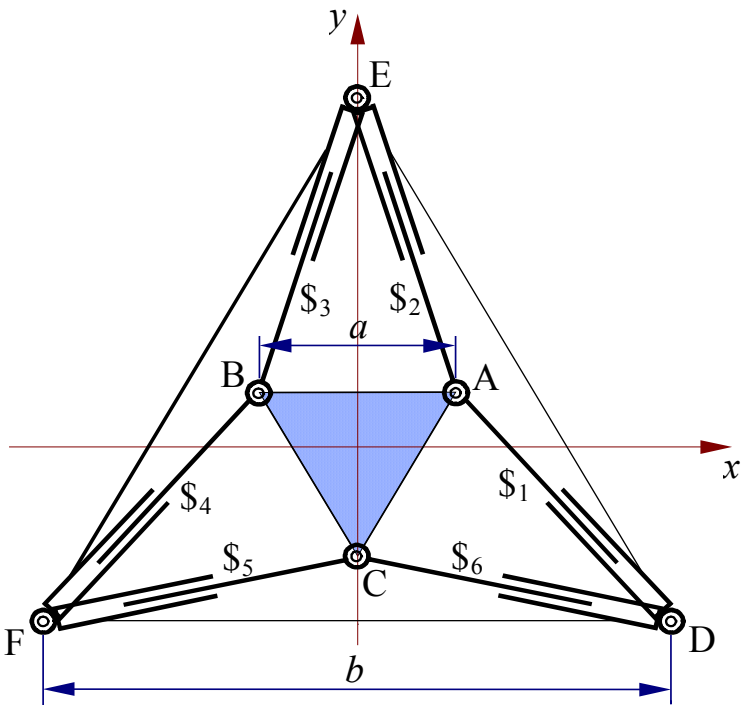

Figure 3: Plan view of 3-3 parallel manipulator

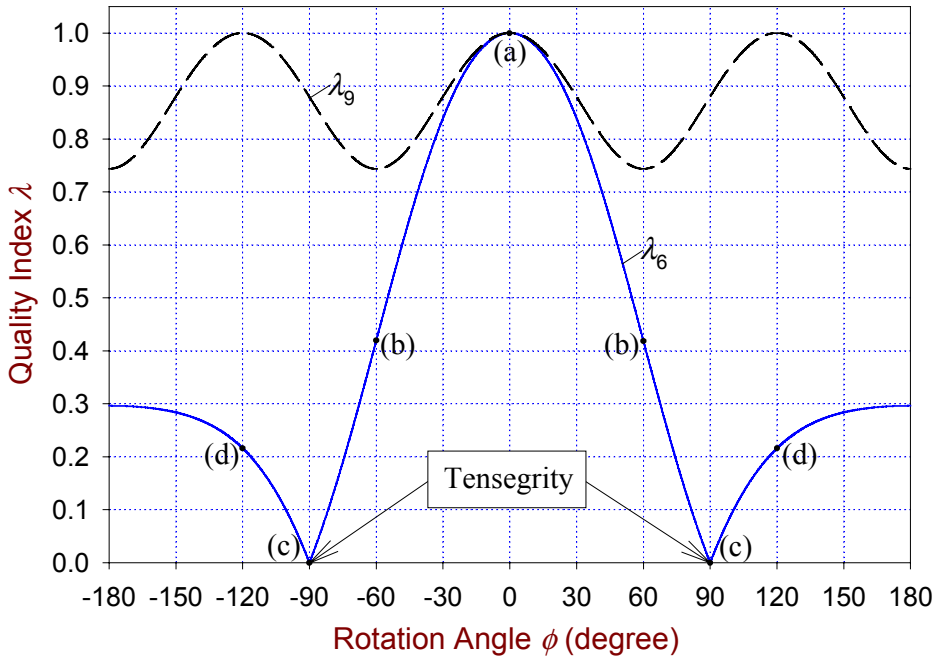

Figure 4: Rotation ϕ about z-axis (octahedral tensegrity prisms, $a = b = h = 1$)

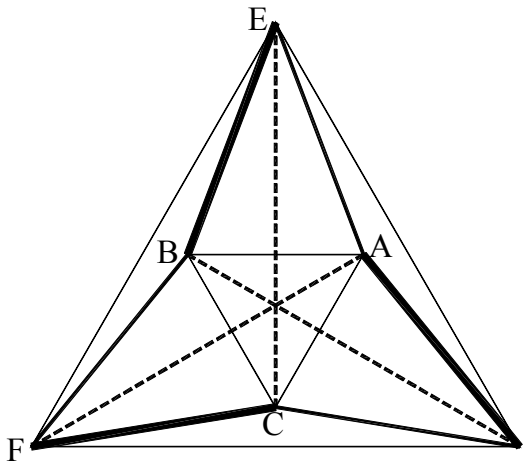

(a) Central Configuration

$\phi = 0°$ $\alpha = -60°$

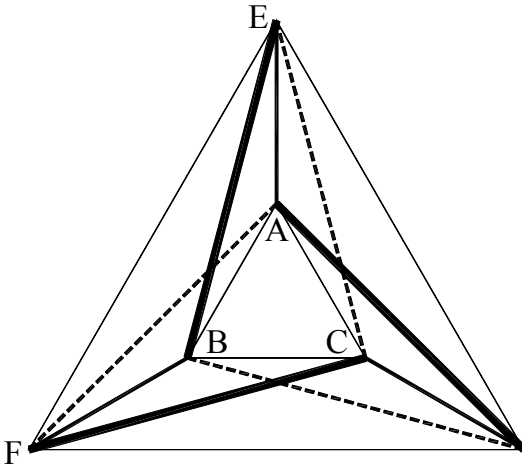

(b) Aligned Configuration

$\phi = 60°$ $\alpha = 0°$

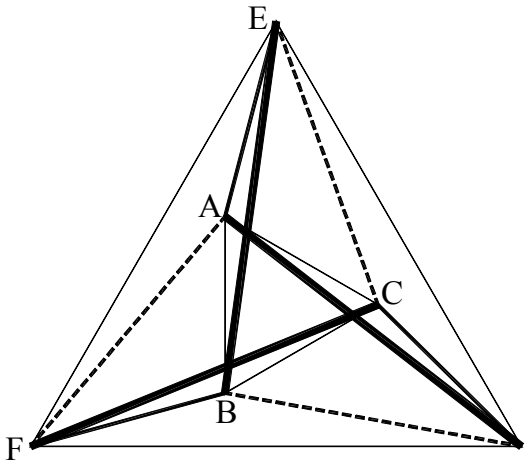

(c) Tensegrity Configuration (special)

$\phi = 90°$ $\alpha = 30°$

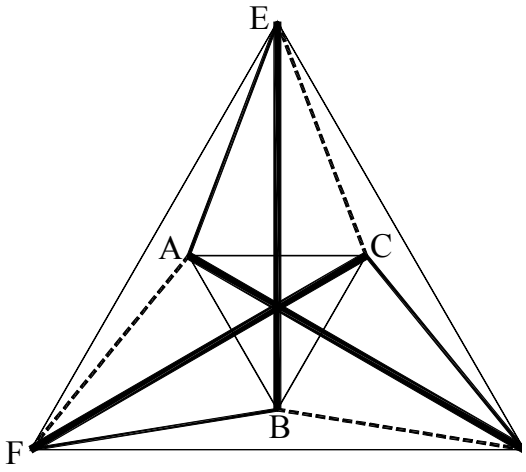

(d) Crossover Configuration (interfere)

$\phi = 120°$ $\alpha = 60°$

Figure 5: Plan view of octahedral tensegrity prisms

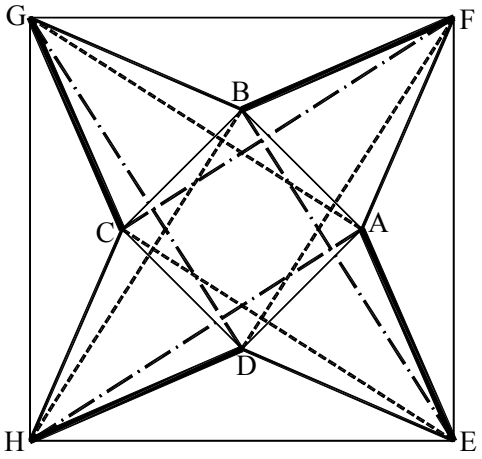

(b) Central Configuration

$\phi = 0°$ $\alpha = -45°$

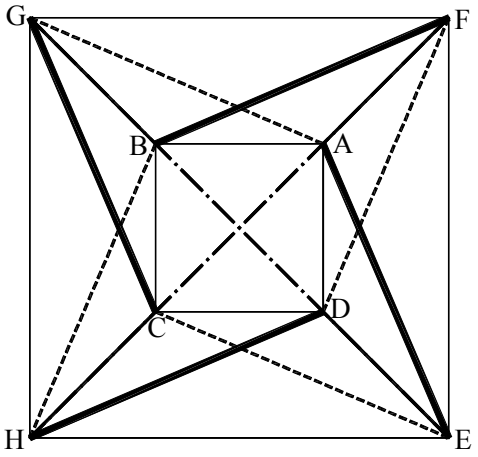

(b) Aligned Configuration

$\phi = 45°$ $\alpha = 0°$

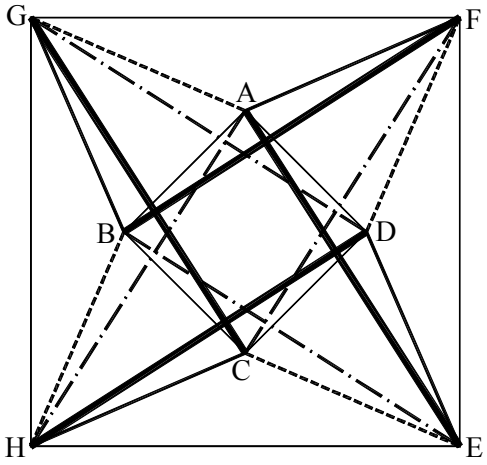

(c) Tensegrity Configuration (special)

$\phi = 90°$ $\alpha = 45°$

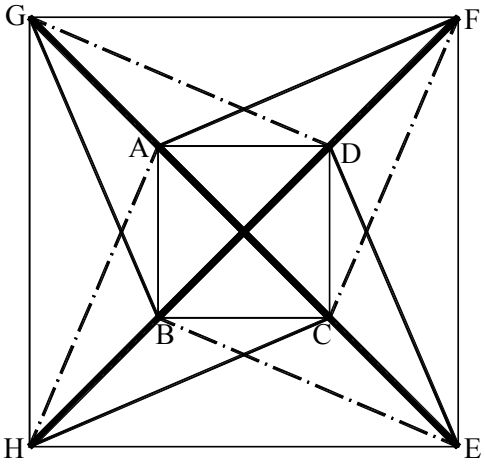

(d) Crossover Configuration (interfere)

$\phi = 135°$ $\alpha = 90°$

Figure 6: Plan view of square tensegrity prisms

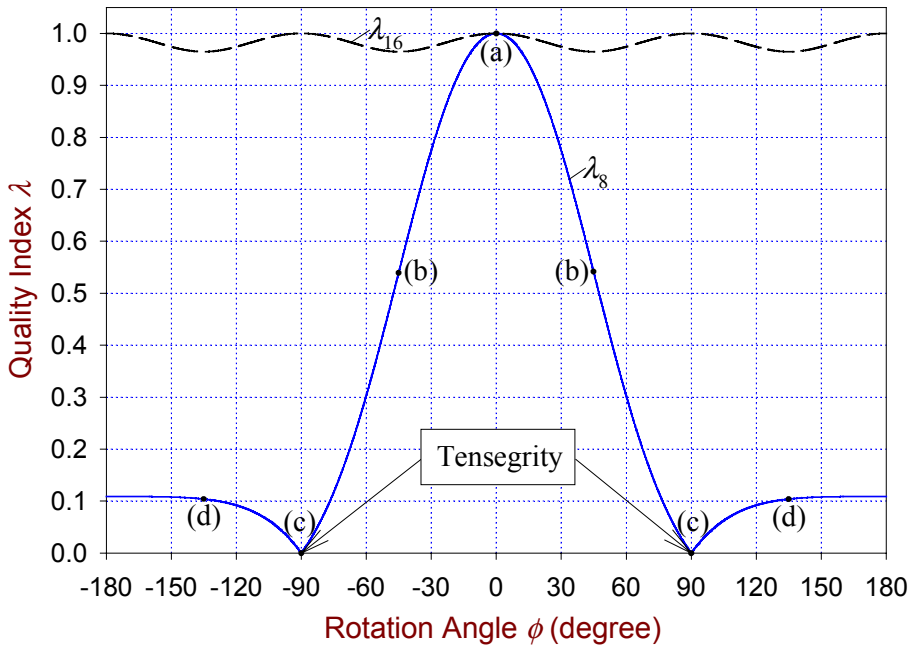

Figure 7: Rotation ϕ about z-axis (square tensegrity prisms, $a = b = h = 1$)

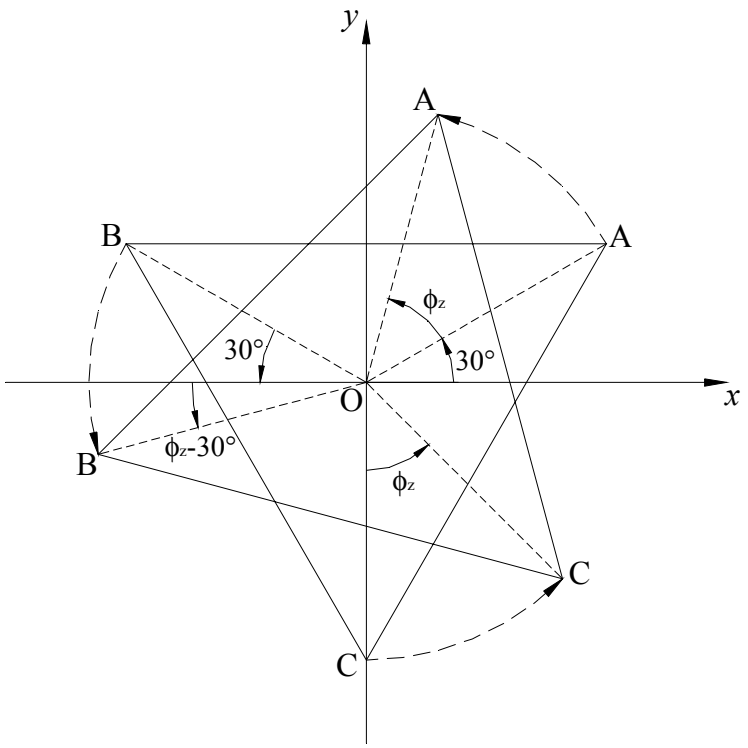

Figure A1: Upper platform rotated through ϕ_z from initial configuration (octahedral tensegrity prisms)

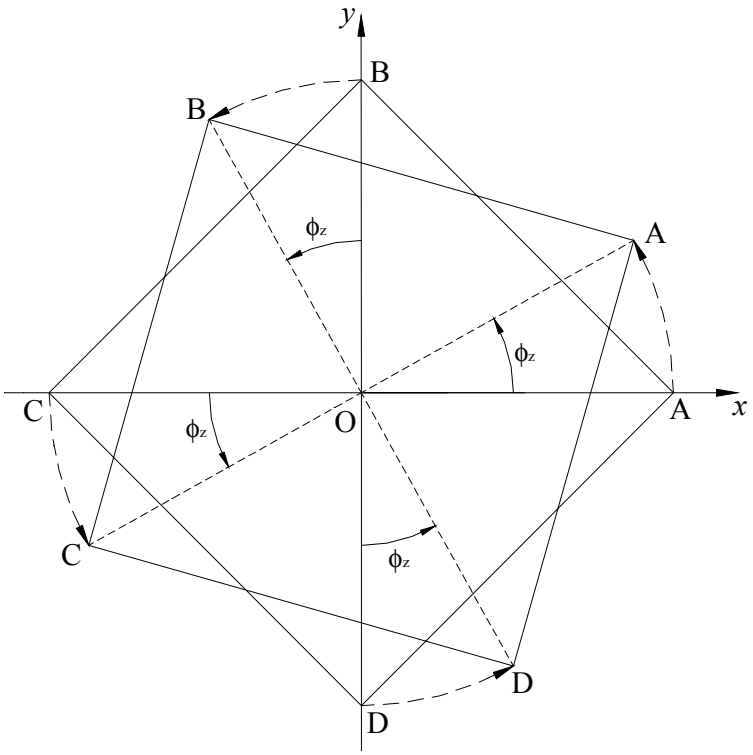

Figure A2: Upper platform rotated through ϕ_z from initial configuration (square tensegrity prisms)